Using capillary forces to determine the elastic properties of mesoporous materials

E. Rolley and N. Garroum

*Laboratoire de Physique Statistique, Ecole Normale Supérieure, UPMC Université Paris 6, Université Paris Diderot,
CNRS, 24 rue Lhomond, 75005 Paris, France*

A. Grosman

Institut des NanoSciences de Paris, CNRS, UPMC Université Paris 6, 4 Place Jussieu, 75005 Paris, France

The capillary forces in mesoporous materials, when imbibed with liquid, are large enough to induce mechanical deformations. Using anisotropic porous silicon, we show that systematic measurements of strain as a function of the pore pressure can yield most of the elastic constants characterizing the porous matrix. The results of this poroelastic approach are in agreement with independent standard stress-strain measurements. The porosity dependence of Young's moduli as well as the values of Poisson's ratios are qualitatively consistent with porous silicon having a honeycomb structure. For a quantitative comparison, we performed finite element modeling of realistic pore geometries. The calculated elastic moduli are found to be much smaller than the measured ones. This is presumably due to both (i) finite-size effects, the Young's modulus of the 5-nm thick walls of the honeycomb could be notably smaller than the Young's modulus of bulk Si, and (ii) defects of the honeycomb structure along the pore axis.

I. INTRODUCTION

The mechanical response of mesoporous materials during fluid adsorption has attracted much interest in recent years, driven by its importance in the context of CO_2 sequestration [1,2] and by other applications such as sensing or actuation [3,4]. Here, we focus on the case where pores are saturated with liquid at pressure P_L. In the limit of elastic deformation, the response of the porous structure to changes in P_L is characterized by the so-called pore-load modulus $M = dP_L/d\epsilon$, a poroelastic coefficient that was introduced by Biot in 1941 [5] in the context of soil mechanics.

In the present work, we use mesoporous silicon (PoSi) as a model system to show how the response to pore pressure can be used to determine the elastic properties of the porous matrix. The validity of this approach, rarely used for anisotropic materials, is demonstrated by comparing these elastic coefficients with the results of ordinary stress-strain tests that we performed independently. We find that the PoSi compliance matrix is consistent with the honeycomb geometry observed in transmission electron microscopy [6] (see Fig. 1). This is in strong contrast with the usual assumption that PoSi is isotropic, which is made in the analysis of nanoindentation experiments [7–10], or the assumption that PoSi has a cubic symmetry, which is made in acoustic velocity measurements [11], either direct or through Brillouin scattering [12].

In the context of mesoporous materials, it was recently proposed that the measurement of the pore-load modulus for porous silica [13,14] and porous silicon [15,16] can yield the effective elastic modulus E^S of the walls forming the solid matrix, provided that the pore geometry is known. Since these walls are only a few nanometers thick, one expects that their effective modulus can be quite different from that of the bulk, similarly to a single nanowire [17] or nanocantilever [18]. The relevance of finite-size effects for mesoporous materials has been recently discussed [19,20], but experimental data are scarce. For mesoporous silica, the wall material (chemical composition, microstructure) depends on the synthesis, so that changes in modulus are difficult to interpret. PoSi is a better candidate since pores are etched in a single crystal, but experiments have reached contradictory results. Gor *et al.* [16] measured the strain transverse to the pore axis for a single sample and concluded that E^S is close to the Young's modulus of bulk silicon. On the contrary, based on strain measurements both transverse and parallel to the pore axis performed on samples with different porosities, we concluded in a previous work that strong finite-size effects exist in the 5-nm-thick silicon walls [15].

In order to clarify this issue, we have performed finite element modeling (FEM) of the PoSi honeycomb geometry, as determined by transverse electron microscopy (TEM). Using bulk silicon properties for the pore walls, the calculated moduli are found to be much smaller than the experimental ones, which is a strong indication of the finite-size effect. However, we also find that the measured moduli are not rescaled by a single factor and that the measured Poisson's ratios are different from those of an ideal honeycomb [21]. This could be due to a small disorder along the pore axis, and this makes it difficult to extract the magnitude of finite-size effects.

II. SAMPLES AND SETUP

Notations. Some experiments have been performed on Vycor, which is an isotropic material. In this case, the response to a pore pressure P_L is characterized by a single pore-load modulus $M \equiv dP_L/d\epsilon$. In contrast, PoSi is an anisotropic material. We note by $\epsilon_\parallel$ the strain parallel to the pore axis ([001] axis); this is called the out-of-plane strain in the honeycomb literature [21]. Due to the underlying cubic symmetry of silicon, the response to P_L is *a priori* different along [100] and [110] axis, but, as discussed below, we could not detect any difference between these two orientations. Hence we note by $\epsilon_\perp$ the strain transverse to the pore axis (or in-plane strain).
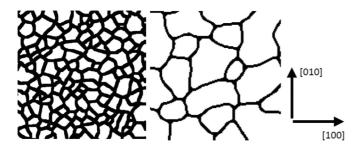
FIG. 1. Binarized TEM images of two porous silicon samples: (left) 50% porosity, (right) 85% porosity, from Ref. [22]. The pores of the honeycomb structure are straight and parallel to the [001] axis. The actual size of the images is $150 \times 150\,\text{nm}^2$.

The response to pore pressure is therefore characterized by two moduli : $M_\parallel = dP_L/d\epsilon_\parallel$ and $M_\perp = dP_L/d\epsilon_\perp$.

Samples. Samples are prepared by electroetching of highly p-doped (100) Si wafers in HF-ethanol solutions. The wafer resistivity lies in the range 0.027–0.033 Ω cm. The resulting porosity is obtained through gravimetry. The mechanical properties depend very strongly on etching conditions, so great care has been taken to use exactly the same etching conditions as for previous samples which were used for the determination of the pore geometry [22]. Pores are straight, nonconnected [23], and perpendicular to the surface wafer, hence along the [001] axis. The pore cross section is irregular and the pore-size distribution is large. Samples with three different porosities p were used (nominal values of 50%, 70%, and 85%) corresponding to mean pore diameter of 12, 26, and 50 nm, respectively. The thickness of the walls separating pores is 5–6 nm, independent of the porosity. Binarized TEM images of the samples are shown in Fig. 1.

The porous layers were studied both detached from the wafer (membranes) or still attached to the underlying Si wafer (supported layers). Samples were used as prepared, at most a few hours after etching, so that the walls are Si-H terminated. The membrane thickness, that is, the sample dimension along the pore axis, was about 65 μm. We checked that 30-μm-thick samples display the same mechanical properties, within experimental reproducibility. The sample dimension transverse to the pore axis was about 25 mm, as only the central part of 2-in. wafers was used in order to avoid possible edge effects.

Experimental setup and protocol were assessed by measuring $M_\perp$ for ten different 50% porosity samples. In the end, we estimate the dispersion to be about 5%. For the other porosities, measurements have been performed on at least two samples. In total, about 30 samples have been analyzed, excluding those which have been rejected because of nonstandard etching parameters.

Direct measurement of transverse properties. Standard stress-strain measurements are performed at room temperature. Rectangular membranes ($10 \times 25\,\text{mm}^2$) are glued at both short ends, one on a fixed frame, the other one on a translation stage submitted to a variable force. $E_\perp$ and $\nu_\perp$ are obtained by measuring optically the strains along both directions of the sample. Note that we have performed numerical calculations of the strain field in order to correct the raw experimental data for the finite aspect ratio of our sample.
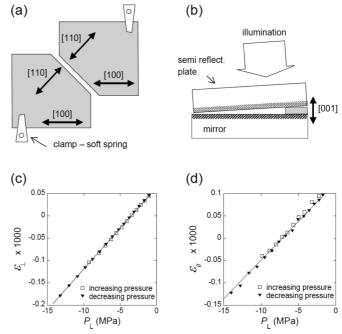

FIG. 2. Schematic view of the setup for transverse (a) and parallel (b) strain measurement. Transverse (c) and parallel (d) strains as a function of the pore pressure P_L for a 50% sample (fluid: heptane).

Principle of pore-load measurement. Samples are held at a regulated temperature (18 °C) in a cell filled with vapor at a pressure P. The fluid is usually n-heptane, but some runs have been performed with ethanol or hexane. First, the samples are saturated with liquid by increasing the vapor pressure almost up to the saturated vapor pressure P_{sat}. Then the gas pressure is ramped up and down at constant rate in a pressure range such that the PoSi remains full of liquid on the so-called saturation plateau [15]. Since no evaporation occurs in the pores, equilibrium is reached very fast.

As long as PoSi is saturated with liquid, we find that the strain varies reversibly and linearly with the pore pressure P_L, which is assumed to be equal to that of a bulk liquid in equilibrium with the vapor: $P_L = \frac{RT}{V_M} \ln(P/P_{sat})$, where R is the ideal gas constant, T the cell temperature, and V_M the liquid molar volume, which is assumed constant.

Measurement of the transverse strain of membranes. Membranes are cut in two pieces with a polygonal shape displaying edges both along [100] and [110] directions. These pieces are clamped on the bottom of the cell, facing each other, so that the free ends of the two pieces form a slit with parallel edges [Fig. 2(a)]. The slit is imaged with a long working distance microscope. Standard image analysis yields a resolution of 50 nm of the slit width, and hence of the sample deformation, the maximum deformation being about 50 μm. Measuring the slit width instead of the position of the free end of a membrane piece automatically cancels any drift of the cell with respect to the lens. As seen in Fig. 2(c), $\epsilon_\perp$ is perfectly linear in P_L and perfectly reversible.

Deformations along the [100] and [110] directions can be measured simply by changing the orientations of the two pieces. [For instance, in Fig. 2(a), the deformation is measured along the [110] axis.] Measuring both deformations

on the same sample allows us to get rid of sample-to-sample variations, which limits the final accuracy on the pore-load modulus.

Measurement of the parallel strain of membranes. The sample size parallel to the pore axis, that is, the thickness of the membranes, is only a few tens of micrometers, three orders of magnitude smaller than the sample size transverse to the pore axis. So the parallel deformation has to be measured using an interferometric setup. A small piece of sample is used as a spacer between a mirror and a semireflecting plate, forming a small-angle wedge [see Fig. 2(b)]. The reflection of a monochromatic beam on the wedge creates interference fringes which shift when the spacer thickness changes. The amplitude of the deformation being of the order of 10 nm, the fringe shift is small, of the order of a tenth of a fringe. The accuracy is limited by thermal drifts. The entire setup, including the CCD camera, is contained in a temperature-controlled box. The fringe shift is corrected for the pressure dependence of the optical index of the gas phase, which we measured prior to the adsorption experiment. As seen in Fig. 2(d), the noise in $\epsilon_\parallel(P_L)$ is larger than in $\epsilon_\perp(P_L)$, but the final uncertainty on the pore-load modulus is still smaller than sample-to-sample variations.

Measurement of the curvature of supported samples. If the PoSi layer is not detached from the underlying wafer, changes in $\epsilon_\perp$ with P_L are small; the main effect of a variation in P_L is to change the transverse stress in the porous layer, which in turn changes the curvature of the bilayer PoSi-Si. The curvature κ of the bilayer can be easily obtained by using the wafer as a mirror in an interferometer and measuring Newton's rings.

Vycor. Complementary experiments have been performed on commercial Vycor samples (Code 7930, Corning, Inc.). Vycor is an isotropic disordered porous silica. The porosity is about 30% and the mean pore diameter is about 5 nm [24]. To remove organic impurities from the pores, the rods were boiled in a 30% solution of hydrogen peroxide for several hours, then rinsed in water. Samples have been cut in a cylindrical rod (diameter 3.8 mm).

For Vycor, the single pore-load modulus was measured with the same setup as used for measuring $\epsilon_\perp$. The fluid was either water or pentane. The Young's modulus was obtained independently by measuring the bending of a rod in a cantilever geometry.

III. COMPLIANCE TENSOR FROM THE RESPONSE TO PORE PRESSURE

Experiments directly yield the pore-load moduli $M_\parallel$ and $M_\perp$. As a first result, systematic measurements of $M_\perp$ do not reveal any dependence with the orientation; the P_L-induced deformations along [100] and [110] axes are the same. Elastic properties appear to be dominated by the random disorder of the honeycomb structure rather than by the underlying cubic symmetry. In the following, we thus assume that PoSi is a transverse isotropic material. On the contrary, $M_\parallel$ and $M_\perp$ values are quite different, especially at high porosity; PoSi appears to be stiffer along the pore axis. Table I summarizes all of the experimental values, which are close to our preliminary measurements [15].

TABLE I. Measured elastic coefficients.

Sample	Porosity p	$E_\perp$ (GPa)	$\nu_\perp$	$M_\parallel$ (GPa)	$M_\perp$ (GPa)	$\frac{d\kappa}{dP_L}$ (GPa^{-1}m^{-1})
50%	0.49	14.6		58	55	16.3
70%	0.70	3.1	0.50	19	11	33.6
85%	0.84	0.57	0.63	7.7	2.8	43.2

Assuming that PoSi is a transverse isotropic material and choosing [100], [010], and [001] as the axes ([001] is the pore axis), the compliance tensor can be written as

$$
\begin{pmatrix} \epsilon_1 \\ \epsilon_2 \\ \epsilon_\parallel \end{pmatrix} = \begin{pmatrix} \frac{1}{E_\perp} & -\frac{\nu_\perp}{E_\perp} & -\frac{\nu}{E_\parallel} \\ -\frac{\nu_\perp}{E_\perp} & \frac{1}{E_\perp} & -\frac{\nu}{E_\parallel} \\ -\frac{\nu}{E_\parallel} & -\frac{\nu}{E_\parallel} & \frac{1}{E_\parallel} \end{pmatrix} \begin{pmatrix} \sigma_1 \\ \sigma_2 \\ \sigma_\parallel \end{pmatrix}, \qquad (1)
$$

where shear components are omitted. Besides $E_\perp$, $E_\parallel$, $\nu_\perp$, and ν, the compliance tensor involves an independent shear modulus.

For a biaxial transverse stress ($\sigma_1 = \sigma_2 = \sigma_\perp$), one has $\epsilon_1 = \epsilon_2 = \epsilon_\perp$. The transverse biaxial modulus $B = E_\perp/(1 - \nu_\perp)$ is defined by $\epsilon_\perp = \sigma_\perp/B$.

A. Transverse biaxial modulus

It is not possible to obtain any engineering elastic constant of the porous matrix from the pore-load moduli $M_\parallel$ and $M_\perp$ *only*, but measuring also the response to pore pressure of supported samples allows us to obtain the biaxial modulus B. Indeed, following [25,26], the curvature dependence $d\kappa/dP_L$ on the liquid pressure reads

$$
\frac{d\kappa}{dP_L} = \frac{2\frac{d\epsilon_\perp}{dP_L}}{\left[d + \frac{1}{3d}\left(\frac{1}{B_{Si}d_{Si}} + \frac{1}{Bd_P}\right)\left(B_{Si}d_{Si}^3 + Bd_P^3\right)\right]}, \qquad (2)
$$

where d_{Si} and d_P are the thicknesses of the two layers and d the total thickness. B_{Si} and B are the biaxial moduli of bulk Si and PoSi, respectively. For [100] wafers, $B_{Si} = 180$ GPa ($E_{\perp Si} = 130$ GPa and $\nu_{\perp Si} = 0.28$ [27]). As shown below, B for PoSi is much smaller. With $d_{Si} \simeq 220$ μm and $d_P \simeq 65$ μm, the term proportional to B/B_{Si} in the bracket in Eq. (2) can be neglected. This leads to

$$
B = M_\perp \frac{d\kappa}{dP_L} \frac{B_{Si}d_{Si}^3}{6d_Pd} \frac{1}{1 - M_\perp \frac{d\kappa}{dP_L} \frac{d}{2}\left(1 + \frac{d_P^2 + d_{Si}^2}{3d^2}\right)}. \qquad (3)
$$

The last factor in the right-hand side of Eq. (3) is a small correction.

In this way, the responses of membranes and of supported samples to pore pressure yield the value of B directly: the knowledge of the pore geometry, and even of the porosity, is not needed. The results for the biaxial modulus are shown in Fig. 3 as a function of the normalized density $1 - p$.

Also plotted in Fig. 3 are B values derived from the measurements of $E_\perp$ and $\nu_\perp$ in direct stress-strain tests. Both determinations of B are consistent within experimental uncertainty. This confirms that the response to the pore pressure provides some of the elastic constants of the porous matrix.
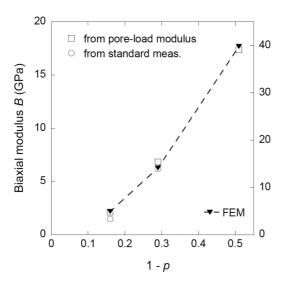
FIG. 3. Transverse biaxial modulus B as a function of the normalized density $1 - p$. Open and closed circles: experimental data (left scale); diamonds: results of finite elements modeling (right scale). The dashed line is only a guide for the eye.

B. Parallel Young's modulus

At first, we consider the isotropic case which is relevant for the Vycor case. When both the pore geometry and the microscopic structure of the solid skeleton are isotropic, the solid strain ϵ is a linear function of the applied hydrostatic stress σ_H and the pore pressure P_L:

$$\epsilon = \frac{1}{3K}\sigma_H + \frac{1}{M}P_L, \qquad (4)$$

where K is the bulk modulus of the porous material at zero (or constant) pore pressure and M the pore-load modulus. In the standard framework of poroelasticity, and under the assumption that the solid phase is homogeneous and isotropic at microscopic scale, it can be shown that [28]

$$\frac{1}{M} = \frac{1}{3K} - \frac{1}{3K^S}, \qquad (5)$$

where K^S is the bulk modulus of the solid phase.

For Vycor, we have measured the pore-load modulus $M = 36.3$ GPa, in agreement with Amberg and McIntosh ($M = 37$ GPa for water [29]) and the Young's modulus $E = 14.5$ GPa, in agreement with Vichit-Vadakan and Scherer ($E = 15.4$ GPa for water [24]). Note that we find the same value of M for pentane and water, within experimental uncertainty. Following [30], we assume that the Poisson's ratio of the porous matrix is 0.16. This gives $K = 7.1$ GPa. From Eq. (5) we find $K^S = 18$ GPa. This bulk modulus for the solid forming the porous matrix is in agreement with the value derived from the study of liquid diffusion due to mechanical stress ($K^S = 19.6 \pm 3.1$ GPa for water [24]). So the knowledge of both the pore-load modulus and the average elastic properties of the porous matrix provides a very simple way to obtain the bulk modulus of the solid phase, as pointed out long ago in the context of rock mechanics [31].

Inversely, for porous silicon, we are looking for properties of the porous matrix. The generalization of Eq. (5) for a

TABLE II. Comparison of the elastic moduli for porous Si obtained from experimental data and calculated for a honeycomb structure. ($\nu_\perp$ for 70% and 85% samples have been calculated for Voronoï honeycomb [21].)

Sample	B (GPa)		$\nu_\perp$		$E_\parallel$ (GPa)		ν	
	Pred.	Exp.	*Pred.*	Exp.	*Pred.*	Exp.	*Pred.*	Exp.
50%	*39.8*	17.4	*0.46*		*66.3*	11	*0.28*	0.39
70%	*13.4*	6.8	*(0.80)*	0.50	*37.3*	6.2	*0.28*	0.33
85%	*4.9*	2.0	*(0.92)*	0.63	*20.4*	2.6	*0.28*	0.33

transverse isotropic material reads [33]

$$\frac{1}{M_\perp} = \frac{1}{B} - \frac{\nu}{E_\parallel} - \frac{1}{3K^S}, \qquad (6)$$

$$\frac{1}{M_\parallel} = \frac{1 - 2\nu}{E_\parallel} - \frac{1}{3K^S}. \qquad (7)$$

Since B, $M_\perp$, and $M_\parallel$ are known, the missing engineering constants $E_\parallel$ and ν can be obtained from these equations provided that K^S is known. As a first guess, neglecting any possible finite-size effects, we choose for K^S the bulk modulus of bulk silicon ($K_{Si} = 97.8$ GPa [27]). Actually, the final values for $E_\parallel$ depend weakly on K^S: a change of K^S by a factor 3 changes $E_\parallel$ by 10% in the worst case (porosity 50%). This has long been recognized: for highly porous materials, the term $1/K^S$ is often negligible compared to $1/K$ in Eq. (5) [31].

The final values for the elastic parameters of PoSi are given in Table II, and $E_\parallel$ is plotted as a function of the normalized density $1 - p$ in Fig. 4. The relative uncertainty in B and $E_\parallel$ is about 15%, and the uncertainty in the Poisson's ratio is 0.02. Thus a complete characterization of the mechanical properties of porous silicon has been obtained.

The values of the transverse moduli are consistent with the early work of Barla *et al.* [25]. By measuring both the lattice mismatch between bulk Si and PoSi and the curvature of supported samples, they obtained for B the following values:
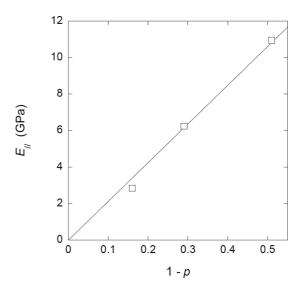

FIG. 4. Parallel Young's modulus $E_\parallel$ as a function of the normalized density $1 - p$.

12 and 8 GPa for 54% and 72% porosity samples, respectively [32].

It is rather difficult to compare with data obtained by other groups as (i) the pore topology of PoSi can be very different from the topology in our sample and/or (ii) PoSi has often been assumed to be isotropic or to have a cubic symmetry. Selecting only reports using PoSi samples etched from highly doped wafers, hence presumably having a honeycomb structure, the reported value of the elastic modulus is about 10 GPa [7,10,12] for a porosity of 70%, which is consistent with our measurements.

IV. GEOMETRY AND ELASTIC PROPERTIES OF THE SILICON WALLS

The next step is to compare the experimental values of elastic constants with what is expected for a honeycomb structure. For a *perfect* honeycomb, that is invariant along the pore axis, $E_\parallel$ and ν are independent of the honeycomb transverse structure: $E_\parallel = (1-p)E^S$ and $\nu = \nu^S$ [21]. The pore axis being here along the [001] axis, it gives: $E_\parallel = (1-p)130$ GPa and $\nu^S = 0.28$ [27]. In contrast, transverse properties are strongly dependent on the pore wall geometry [21]. Few studies are devoted to random honeycomb, and, to our knowledge, they are restricted to Voronoï honeycomb [34,35], often in the limit of low-density materials. We have thus performed FEM for "real" PoSi structures, i.e., as reconstructed from TEM images: the transverse structure is well described, but we neglect disorder along the pore axis and assume a perfect honeycomb structure.

Finite element modeling. Since the pore length is 3 orders of magnitude larger than the typical transverse dimension of the pores, we performed a two-dimensional (2D) calculation in the transverse plane. To limit edge and finite-size effects, we use large systems consisting of roughly 1000 pores. The mesh is irregular because of the randomness of the honeycomb, the typical mesh size being 1 nm. This is not very small compared to the wall thickness (5–6 nm), but we checked that using a mesh size 2 times smaller does not change the deformation by more than a few percent. In the calculation, the material properties of the walls were that of silicon single crystal with the same orientation as real samples ([001] axis parallel to the pore axis).

In order to obtain the transverse biaxial modulus, the same stress σ_{ext} is applied on the boundary in [100] and [010] directions [36]. Calculations are done with COMSOL software in the "plane stress" condition, that is, imposing a zero parallel stress. Rather than the displacement of the system boundary, we measure the average radial displacement u from the center of the system. We find u to increase linearly with the distance r to the center for r smaller than half the system size, the transverse strain is then defined as du/dr and $B = \sigma_{ext}/(du/dr)$. As a test, we have performed simulation for regular hexagonal honeycombs and we recover the classical result at low density [21]. We find that the disorder in PoSi leads to a strong reduction in B compared to a hexagonal honeycomb. We hypothesize that this is due to the bending of walls in PoSi structures, which does not occur in a periodic structure submitted to a biaxial stress.

Predicted and experimental values are gathered in Table II. FEM results for B are also plotted in Fig. 3. PoSi, especially at low density, presents the generic features of a honeycomb structure: a Young's modulus smaller in the transverse than in the parallel direction, and a large transverse Poisson's ratio. Let us make a few detailed comments about our findings:

(1) The calculated and measured density dependence of B are very similar (B varies roughly like $(1-p)^2$), but the calculated value is about 2.3 times larger. This is an indication that the elastic modulus of the walls is reduced compared to that of bulk Si. Finding such a strong reduction is not very surprising for a system where the walls are a few nanometers thick. It is well known from experiments performed on nanowires or nanocantilevers that finite-size effects decrease the effective Young's modulus [17,18,37], and a reduction by a factor 3 has already been observed for a 12-nm-thick cantilever etched in crystalline silicon [18].

(2) The calculated and measured density dependence of $E_\parallel$ are the same ($E_\parallel \propto (1-p)$), but the calculated value is now larger than the measured one by a factor 6. Here, it seems unlikely that finite-size effects alone can be responsible for such a strong variation. Rather, we think that PoSi samples are softer than expected along the pore axis because the PoSi is not a perfect honeycomb. Indeed, TEM pictures reveal defects of the pore walls which are not taken into account in 2D FEM. Presumably, these defects trigger wall bending when the structure is submitted to uniaxial stress along the pore axis, which would lead to a strong decrease in the parallel Young's moduli.

(3) For a perfect honeycomb, the Poisson's ratio ν is constant while $\nu_\perp$ increases with the porosity, up to 1 in the limit of 100% porosity [21]. The experimental values approximately satisfy these properties, although $\nu_\perp$ is smaller than expected. Indeed, calculated values of $\nu_\perp$ are always found to be larger than 0.9 for 85% porosity, and, moreover, to be very weakly dependent on the transverse geometry [34,35]. Thus, the difference between experimental and theoretical values probably does not stem from a poor model for the transverse geometry but rather from the noninvariance parallel to the pore axis.

(4) Finally, one should be aware that "experimental" values of ν are slightly dependent on the choice of K^S in Eq. (6). For instance, dividing K^S by a factor of 2 with respect to bulk silicon leads to a Poisson's ratio almost independent of the porosity ($\nu \simeq 0.3$).

To summarize, the qualitative behavior of moduli and Poisson's ratios is consistent with a honeycomb structure, but there is a quantitative disagreement between experiments and FEM despite our efforts to take into account the structure of PoSi. In particular, we find that measured elastic moduli of the porous matrix are much smaller that expected. This is a strong indication that the Young's modulus E^S of the 5–6-nm-thick walls is smaller than that of bulk silicon. However, one cannot reconcile FEM and experiment by simply rescaling E^S. It is very likely that the noninvariance of the structure along the pore axis also contributes to the decrease of the moduli, especially $E_\parallel$. In the present stage of modeling, it is not possible to disentangle the effects of nonideality of the structure and of the finite size of the walls. Finally, note that

defects along the pore axis could also impact the transport properties along the pore, which have been recently measured [38].

It is interesting to come back to ordered nanoporous silicas, as these systems are exactly the opposite of PoSi: the pore structure is simple but the microstructure and the very nature of the solid is often not completely known. For MCM-41, Prass *et al.* [13] have performed a simple analysis of $M_\perp$, without considering parallel strain, and inferred that the bulk modulus of the walls is 88 GPa while the Young's modulus for bulk silica is 72 GPa. The difference was attributed to a higher portion of small siloxane rings in thin walled nanoporous silica as compared to fused silica. The same analysis for SBA-15 yields 35 GPa, the difference with respect to bulk silica being now attributed to the microporosity of silica walls. Finally, let us mention that for disordered nanoporous silica (Vycor) we find $K^S = 18$ GPa, which is twice smaller than K^S for bulk silica. For Vycor, this low value was attributed to the presence of hydroxyl groups [30]. So, the response to pore pressure provides a measurement of the Young's modulus of silica nanowalls, but this modulus is system dependent, which prevents concluding unambiguously about any finite-size effect.

V. CONCLUSION

Using porous silicon, we have shown that, in a saturated mesoporous material, the analysis of the response to pore pressure yields elastic constants in agreement with direct stress-strain tests. The standard framework of poroelasticity has allowed us to determine the full set of PoSi elastic constants, with the exception of one shear modulus, for various porosities. The knowledge of the mechanical properties of the matrix has practical purposes, for instance, in the design of microelectromechanical systems devices or acoustic superlattices with porous silicon [12].

From a more fundamental point of view, it is important to determine whether the elastic properties of the nanometric solid walls differ from the bulk properties. PoSi, which is a single crystal, is *a priori* a good system since the nature of the walls is perfectly known. However, its complex structure precludes a quantitative conclusion regarding finite-size effects: it is likely that noninvariance along the pore axis has a strong impact on the elastic properties of the porous matrix, especially on $E_\parallel$. Obtaining wall properties from those of the matrix first requires to determine the pore geometry with a very high resolution, better than in available data [6], and second requires a full three-dimensional FEM. This is a difficult task; a first step would be to study to what extent a modulation of the pore size and/or wall thickness can account for the measured values of $E_\parallel$ and $\nu_\perp$. Another way to separate the contributions of the wall properties and of the pore geometry would be to perform a mild oxidation in order to change the hydrogen to an hydroxyl termination. This would presumably modify the effective modulus of the Si walls [37,39] without changing the pore geometry very much.

[1] A. Busch and Y. Gensterblum, Int. J. Coal Geology **87**, 49 (2011).

[2] S. Nikoosokhan, M. Vandamme, and P. Dangla, J. Mech. Phys. Solids **71**, 97 (2014).

[3] L. Bertinetti, F. D. Fischer, and P. Fratzl, Phys. Rev. Lett. **111**, 238001 (2013).

[4] Q. Zhao, J. W. C. Dunlop, X. Qiu, F. Huang, Z. Zhang, J. Heyda, J. Dzubiella, M. Antonietti, and J. Yuan, Nat. Commun. **5**, 4293 (2014).

[5] M. A. Biot, J. Appl. Phys. **12**, 155 (1941).

[6] A. Grosman and C. Ortega, in *Structural and Optical Properties of Porous Silicon Nanostructures*, edited by G. Amato, C. Delerue, and H. J. von Bardeleben (Gordon and Breach Science Publishers, London, 1997), Chap. 11, pp. 317–331.

[7] D. Bellet, P. Lamagnère, A. Vincent, and Y. Bréchet, J. Appl. Phys. **80**, 3772 (1996).

[8] C. A. Charidis, A. Skarmaoutsou, A. G. Nassiopoulou, and A. Dragoneas, Mater. Sci. Eng. A **528**, 8715 (2001).

[9] M. Oisten and P. Bergstrom, Phys. Status Solidi A **206**, 1278 (2009).

[10] Z. Fang, M. Hu, W. Zhang, X. Zhang, and H. Yang, Thin Solid Films **517**, 2930 (2009).

[11] G. N. Alliev, B. Goller, and P. A. Snow, J. Appl. Phys. **110**, 043534 (2011).

[12] A. M. Polomska-Harlick and G. T. Andrews, J. Phys. D **45**, 075302 (2012).

[13] J. Prass, D. Müter, P. Fratzl, and O. Paris, Appl. Phys. Lett. **95**, 083121 (2009).

[14] M. Schoen, O. Paris, G. Günther, D. Müter, J. Prass, and P. Fratzl, Phys. Chem. Chem. Phys. **12**, 11267 (2010).

[15] A. Grosman, J. Puibasset, and E. Rolley, Europhys. Lett. **109**, 56002 (2015).

[16] G. Y. Gor, L. Bertinetti, N. Bernstein, T. Hofmann, P. Fratzl, and P. Huber, Appl. Phys. Lett. **106**, 261901 (2015).

[17] Y. Zhu, F. Xu, Q. Qin, W. Y. Fung, and W. Lu, Nano Lett. **9**, 3934 (2009).

[18] X. Li, T. Ono, Y. Wang, and M. Esashi, Appl. Phys. Lett. **83**, 3081 (2003).

[19] M. Liu, J. Wu, Y. Gan, and C. Q. Chen, AIP Adv. **6**, 035324 (2016).

[20] X. Feng, R. Xia, X. Li, and B. Li, Appl. Phys. Lett. **94**, 011916 (2009).

[21] L. J. Gibson and M. F. Ashby, *Cellular Solids: Structure and Properties* (Pergamon Press, New York, 1988).

[22] A. Grosman and C. Ortega, Langmuir **24**, 3977 (2008).

[23] B. Coasne, A. Grosman, C. Ortega, and M. Simon, Phys. Rev. Lett. **88**, 256102 (2002).

[24] W. Vichit-Vadakan and G. W. Scherer, J. Am. Ceram. Soc. **83**, 2240 (2000); **87**, 1614(E) (2004).

[25] K. Barla, R. Herino, G. Bomchil, and J. C. Pfister, J. Cryst. Growth **68**, 727 (1984).

[26] F. K. Reinhart and R. A. Logan, J. Appl. Phys. **44**, 3171 (1973).

[27] M. A. Hopcroft, W. D. Nix, and T. W. Kenny, J. Microelectromech. Syst. **19**, 229 (2010).

[28] E. Detournay and A. H. D. Cheng, in *Comprehensive Rock Engineering: Principles, Practice and Projects*, edited by

C. Fairhurst (Pergamon Press, New York, 1993), Vol. 2, pp. 113–171.

[29] C. H. Amberg and R. McIntosh, Can. J. Chem. **30**, 1012 (1952).

[30] G. W. Scherer, J. Am. Ceram. Soc. **69**, 473 (1986).

[31] A. Nur and J. D. Byerlee, J. Geophys. Res. **76**, 6414 (1971).

[32] The value of the biaxial modulus can be derived from the work of Barla *et al.* by using their experimental values in Table 1 and Eq. (6) in Ref. [25]. In their paper, the authors rather give the value of the Young's modulus, but their derivation is based on a supplementary hypothesis for the Poisson's ratio that is contradictory with the present work.

[33] A. H.-D. Cheng, Int. J. Rock Mech. Min. Sci. **34**, 199 (1997).

[34] M. J. Silva, W. C. Hayes, and L. J. Gibson, Int. J. Mech. Sci. **37**, 1161 (1995).

[35] H. X. Zhu, J. R. Hodbell, and A. H. Windle, J. Mech. Phys. Solids **49**, 857 (2001).

[36] Following Gor *et al.* [16], we have also determined the 2D-transverse pore modulus $M_{\perp,2D}$ by measuring the transverse strain when, instead of applying an external stress, the inner surfaces of the pores are submitted to a fluid pressure P_L. However, one should be aware that $M_{\perp,2D}$ cannot be directly compared to the experimental value since the condition along the parallel axis is different in the experiment and in the numerics. When the parallel stress and strain are properly taken into account, the Gor approach yields the same biaxial modulus as the standard calculation.

[37] H. Sadeghian, F. van Keulen, and H. Goosen, in *Advances in Micro/Nano Electromechanical Systems and Fabrication Technologies*, edited by K. Takahata (InTech, Rijecka, Croatia, 2013), Chap. 7, pp. 155–186.

[38] J. Puibasset, P. Porion, A. Grosman, and E. Rolley, Oil Gas Sci. Technol. **71**, 54 (2016).

[39] J. Wang, Q. Huang, and H. Yu, Solid State Commun. **145**, 351 (2008).